

3KG: Contrastive Learning of 12-Lead Electrocardiograms using Physiologically-Inspired Augmentations

Bryan Gopal *

Ryan W. Han *

Gautham Raghupathi *

Andrew Y. Ng

Geoffrey H. Tison †

Pranav Rajpurkar †

BRYANG@CS.STANFORD.EDU

RYANHAN@CS.STANFORD.EDU

GAUTHAM@CS.STANFORD.EDU

ANG@CS.STANFORD.EDU

GEOFF.TISON@UCSF.EDU

PRANAVSR@CS.STANFORD.EDU

Abstract

Self-supervised contrastive learning approaches leverage modality-specific context or invariances to pretrain models using unlabeled data. While contrastive learning has demonstrated promising results in the image domain, there has been limited work on determining how to exploit modality-specific invariances in biosignals such as the electrocardiogram. In this work, we propose 3KG, a method to generate positive pairs for contrastive learning using physiologically-inspired 3D augmentations of the 12-lead electrocardiogram. We evaluate representation quality by fine-tuning a linear layer for the downstream task of 24-class diagnosis on the PhysioNet 2020 challenge training data, and find that models trained with physiologically-inspired augmentations both outperform and complement standard time-series augmentations. Our best performing strategy, which incorporates spatial rotation, spatial scaling, and time masking, achieves a performance increase of 0.16, .086, and .046 in mean AUROC over a randomly initialized baseline at 1%, 10%, and 100% label fractions respectively. Additionally, we show that the strength of spatial augmentations does not significantly affect the quality of the learned representations. Finally, we investigate the clinical relevance of how physiologically-inspired augmentations affect the performance of our classifier on different disease subgroupings. As expert annotations are often expensive and scarce for medical contexts, our approach highlights the potential of machine learning to tackle medical problems with large quantities of unlabeled biosignal data by exploiting their unique biological properties.

* Equal Contribution

† Equal Contribution

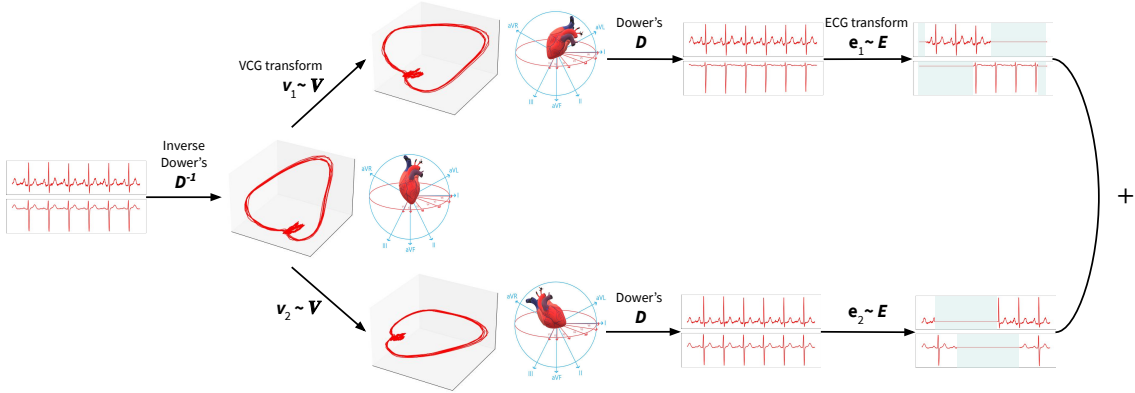


Figure 1: **3KG Overview.** Positive pairs for contrastive learning are generated by composing stochastic augmentations of the 12-lead ECG in the VCG and ECG spaces. Only leads II and V2 are shown for the sake of simplicity.

1. Introduction

Self-supervised learning approaches leverage unlabeled data to pretrain models for subsequent fine-tuning on downstream tasks in a low-label regime (Hjelm et al., 2019; Wu et al., 2018). Within this paradigm, contrastive learning approaches such as SimCLR, MoCo, and BYOL have recently risen in prominence for computer vision tasks (Chen et al., 2020a,b; He et al., 2020; Chen et al., 2020c; Grill et al., 2020). However, there is only limited work on determining how contrastive learning algorithms can be applied to the medical signal analysis domain (Kiyasseh et al., 2020a; Cheng et al., 2020; Kiyasseh et al., 2020b).

The 12-lead electrocardiogram (ECG) is a noninvasive, commonly obtained test important to screening, diagnosis, and management of various cardiovascular conditions (Salerno et al., 2003; Fesmire et al., 1998). ECG interpretation is typically carried out by physicians who are trained to make diagnoses based on unique abnormalities in a subset of the 12 leads (Anh et al., 2006; Bond et al., 2014; Hurst, 2000; Cairns et al., 2017). There are a large number (> 100) of existing ECG diagnoses, and recent studies have demonstrated the ability of machine learning methods to make novel diagnoses beyond those traditionally made with ECGs (Tison et al., 2019; Attia et al., 2019b,a).

Self-supervised contrastive learning presents a promising avenue for improving the performance and label-efficiency of ECG interpretation strategies. In contrastive learning, the loss function dictates that representations of positive pairs (samples with shared context) should be similar while representations of negative pairs (samples without shared context) should be dissimilar. The selection of pairs thus controls the information contained in the learned representations, with good positive pairs containing minimal mutual information apart from that necessary for the downstream task (Tian et al., 2020).

In this work, we propose a method of producing positive pairs using ECG-specific 3D transformations in the vectorcardiogram space to improve the quality of representations

learned by contrastive learning. 12-lead ECGs capture cardiac electrical activity derived from the heart in 3-dimensional space. Vectorcardiograms, which can be derived from the ECG data, specifically represent this electrical activity along three orthogonal spatial axes (x,y,z) as a series of vectors tracing contours around a central point over time. We evaluate the quality of pretrained representations for the downstream task of ECG diagnosis on the PhysioNet 2020 Challenge dataset. Our contributions are as follows:

1. From a technical perspective, we introduce a family of 3D augmentations for 12-lead ECGs. Based on the observation that natural variability in cardiac structure and orientation exists without substantive clinical implications, we hypothesize that ECGs are invariant to minor spatial perturbations of the heart’s 3D electrical activity (Olivetti et al., 1995; Einthoven et al., 1950; Kashou et al., 2020). We provide an intuition for this invariance in Figure 1.
2. From an experimental perspective, we show that our approach improves over and complements standard time-series augmentations. Additionally, we show that the strength of spatial augmentations does not significantly affect the quality of the learned representations.
3. From a medical perspective, we investigate the clinical relevance of how physiologically-inspired augmentations affect the performance of our classifier on different disease subgroupings.

Generalizable Insights about Machine Learning in the Context of Healthcare

In this work, we explore how contrastive learning can be applied to ECG signal data by exploiting properties of the physiological phenomena they represent. We show that even at low label fractions, the representations learned by our method allow us to build a highly discriminative classifier. As expert annotations are often expensive and scarce for medical contexts, our approach highlights the potential of machine learning to tackle medical problems with large quantities of unlabeled biosignal data by exploiting their unique biological properties.

2. Related Work

Contrastive learning approaches leverage the intuition that positive pairs (samples with shared context) should have similar latent representations while negative pairs (samples without shared context) should have dissimilar representations (Tian et al., 2020). In the image domain, Tian et al. (2019) propose using different modal views of an image as positive pairs. More recently, Chen et al. (2020a) and He et al. (2020) exploit invariances in images by defining positive pairs as differently augmented views of the same image. Chen et al. (2020a) note that augmentation strength and composition are crucial for learning good representations. However, Kiyasseh et al. (2020a) find that traditional augmentations used for contrastive learning in computer vision (i.e. Gaussian noise, axis flipping) do not perform well when applied in the ECG domain.

Instead, the authors propose to define positive pairs at the levels of different modal views (multi-lead and multi-segment) of a recording, different recordings originating from

the same patient, or different patients with similar patient attributes respectively (Kiyasseh et al., 2020a,c,b). Similar to Tian et al. (2019), these methods incorporate domain-specific context to define commonalities between views but fall short of exploiting invariances in the data signal itself.

Alternatively, Sarkar and Etamad (2019) and Cheng et al. (2020) attempt to exploit invariances in temporal signals by applying signal transformations such as bandstop filtering and time warping for a transformation prediction pretext task and for contrastive learning respectively. These methods are most similar to our work in that they exploit invariances inherent to the ECG signal for self-supervised learning. In contrast to methods which extend classic time-series augmentations to the ECG domain, we present and validate a system of physiologically-inspired augmentations for contrastive learning of 12-lead ECGs.

3. Methods

3.1. Dataset

All experiments were run on the PhysioNet 2020 challenge training data (Alday et al., 2020). The dataset consists of 12-lead ECG recordings from four data sources with various distributions of patient characteristics, recording length, and diagnoses. There are a total of 43,134 recordings which we split into training, validation, and test sets in an 80/10/10 configuration. The training set was further divided into 1%, 10%, and 100% label fraction splits to simulate label scarcity for the downstream task. Labels are at the recording level, and each recording could be associated with multiple labels. Although the training data had 111 classes present, we chose to classify only the 27 SNOMED CT codes that were included in the challenge evaluation metric. Additionally, we coalesced the following SNOMED CT labels after a cardiologist determined the diagnoses to be substantially equivalent: Complete right bundle branch block (713427006) and right bundle branch block (59118001), premature atrial contraction (284470004) and supraventricular premature beats (63593006), and premature ventricular contractions (427172004) and ventricular premature beats (17338001). Our final downstream task was thus 24-class multilabel classification.

3.2. Preprocessing

To ensure ECGs from different sources were standardized, all recordings were resampled to 500 Hz and then exhaustively cropped into disjoint 5-second segments. All crops were tagged with the file they originated from for later use in loss computation. ECGs were normalized to unit range, but were not translated so as to maintain the isoelectric line at 0.

3.3. Generating positive pairs for contrastive learning with 3D augmentations

Given an unlabeled sample x and a set of augmentations \mathcal{T} , our goal during pretraining is to learn a parametrized encoder f_θ to minimize the InfoNCE loss

$$\mathcal{L}(x) = -\log \frac{\exp[f_\theta(x_1) \cdot f_\theta(x_2)/\tau]}{\sum_{i=1}^{2K} \exp[f_\theta(x_1) \cdot f_\theta(z_i)/\tau]} \quad (1)$$

where positive pair $(x_1 = t_1(x), x_2 = t_2(x))$, $t_1, t_2 \in \mathcal{T}$ are stochastically augmented views of the input x , and negative pairs (x_1, z_i) , $1 \leq i \leq 2K$ are augmentations of different samples with z_i coming from the batch of size K (van den Oord et al., 2018). Loss is computed and averaged across all positive pairs in a batch, with τ denoting a temperature hyperparameter that controls for the extremity of the softmax function.

In order for the encoder to learn features useful for ECG diagnosis, the family of transformations \mathcal{T} should preserve spatiotemporal features relevant for clinical assessment of cardiovascular conditions. To this end, we propose 3KG, a system of physiologically-inspired transformations for contrastive learning that respect the spatiotemporal invariances required to make diagnoses on 12-lead ECGs. In particular, we define

$$\mathcal{T} = \mathcal{E} \circ \mathcal{V}$$

where \mathcal{E} is the set of all ECG augmentations and \mathcal{V} is the set of all 3D perturbations such that

$$\mathcal{V}(x) = DSRD^{-1}x,$$

where $D^{-1} \in \mathbb{R}^{3 \times 12}$ projects the 12-lead ECG into a 3-dimensional vectorcardiogram (VCG), $R \in \mathbb{R}^{3 \times 3}$ is a rotation matrix, $S \in \mathbb{R}^{3 \times 3}$ is a scaling matrix, and $D \in \mathbb{R}^{12 \times 3}$ projects the VCG back into the ECG space. As described, vectorcardiograms represent the electrical activity of the heart along three orthogonal spatial axes (x,y,z) as a series of vectors tracing contours around a central point over time. We use the Dower and Inverse Dower linear transformations to convert between ECGs and VCGs (Jaros et al., 2019). However, because VCGs exist in a lower-dimensional space than ECGs, the linear conversion process observes some loss due to the fact that D approximates an inverse to the underdetermined system D^{-1} .

3.4. Augmentation module

During pretraining, we randomly sample a batch of K crops and produce the pairs of augmented examples derived from the batch, resulting in $2K$ augmented crops. We apply our augmentation scheme in the following order:

1. VCG Augmentations

- (a) **Random Rotation.** We rotate the VCG on all three axes in a random order, where the per-axis rotation is a random value sampled from a uniform distribution between $-r$ to $+r$ degrees.
- (b) **Random Scale.** We scale the VCG on all three axes, where the per-axis scale is a random value sampled from a uniform distribution between $[1, s]$ with a 50% probability of inversion. This means that on average, one half of the scale factors is between $[1/s, 1]$ and the other half is between $[1, s]$.

2. ECG Augmentations

- (a) **Random Time Masking.** We sample 1 time step for each lead as a starting index, and replace the subsequent $\lfloor L \cdot p_t \rfloor$ time steps to be zero over all leads (wrapping around to the beginning of the recording as necessary), where L is the

number of time steps in the sample and $0 \leq p_t \leq 1$ is the user-specified maximum time mask percentage.

Taking significant inspiration from self-supervised approaches in speech recognition (Baevski et al., 2020), our augmentations in item 2a are motivated by the fact that trained cardiologists often only need a single beat on a single lead to ascertain a significant portion of ECG diagnoses. As such, a self-supervised model should operate with augmentations that allow it learn to generate useful representations even with a high percentage of data masked. Moreover, random time masking come with the added benefit of never introducing distortions into an ECG that invalidates the accuracy of its given diagnosis labels.

3.5. Encoder and Embedding Aggregation

Our encoder is a 1-D convolutional neural network with a single channel input and 256-dimensional output. Following similar work in self-supervision, we leveraged a 3-layer MLP head in pretraining that projected this 256-dimensional output into 128-dimensional space (Chen et al., 2020a). We chose to use 1 input channel and process each lead separately to increase the versatility of our model to settings where not all 12 leads are available, such as in the ambulatory (Holter) setting where the standard of care is a single lead ECG (Kennedy, 1992). To compute a representation for a 12-lead ECG crop, single lead embeddings across all leads were averaged along the channel dimension. We used the Adam optimizer with a learning rate of 1×10^{-3} and a batch size of 512 for all pretraining experiments (Kingma and Ba, 2017).

3.6. Evaluation on downstream task

Following the work of SimCLR, we drop the last two layers of our MLP once pretraining is done, conducting our downstream experiments using the embeddings produced by the first MLP layer (Chen et al., 2020b). We attach a single linear layer to classify the output of our encoder f_θ . We directly evaluate the quality of the representations learned by the feature encoder by freezing f_θ and training the single linear layer to predict diagnosis labels. Models were trained using a binary cross-entropy loss averaged over all classes, and we report the mean per-class AUROC for the test set in all experimental results. We used the Adam optimizer (Kingma and Ba, 2017) with a learning rate of 1×10^{-3} and a batch size of 512 for all downstream experiments.

3.7. Determining Statistical Significance

We evaluate the statistical significance each of our experiments against a stated baseline model using a bootstrapping setup. We randomly sample n test set predictions with replacement (where n is the size of the test set) from both the baseline and the model of interest. We then calculate the AUROC difference between the two resampled prediction sets. We repeat this entire process 500 times, and construct a 95% confidence interval using all the resulting differences. If 0 lies outside this interval, we consider the model of interest to be significantly different than the baseline model.

4. Results

4.1. Spatial VCG Augmentations

Method	PhysioNet 2020 (AUROC)		
	1% ($\mu \pm \sigma$)	10%	100%
<i>Baseline</i>			
Random	0.549 ± 0.044	0.709	0.760
Time mask	0.684 ± 0.012	0.765	0.799
<i>Single Augmentations</i>			
Rotate	$0.703 \pm 0.011^*$	0.767	0.785
Scale	0.668 ± 0.014	0.738	0.769
<i>Combined Augmentations</i>			
Rotate + Time mask	$0.713 \pm 0.016^*$	0.786*	0.800
Scale + Time mask	0.682 ± 0.018	0.775*	0.798
Rotate + Scale	$0.690 \pm 0.015^*$	0.752	0.775
Rotate + Scale + Time mask	$0.709 \pm 0.019^*$	0.795*	0.806*

Table 1: **Augmentation ablation study.** * denotes statistically significant improvement over time mask. Experiments at the 1% fraction were run across 5 randomly drawn splits to provide an understanding of the model’s variable performance. Rotation was applied with parameter $r = 5^\circ$ and scaling was applied with parameter $s = 1.1$.

4.1.1. SINGLE SPATIAL AUGMENTATION

We observe that Rotate outperforms our baseline of time masking across 2 out of 3 of our label fractions and that Scale under performs our baseline across all 3 label fractions. While rotate outperforms time mask at the 1% (0.703 vs 0.684) and 10% (0.767 vs 0.765) label fractions, the difference is only statistically significant at the 1% label fraction. At the 100% label fraction, Time Mask (0.799) outperforms Rotate (0.785). We find that Scale performs worse than Time Mask at the 1% (0.668 vs 0.684), 10% (0.738 vs 0.765), and 100% (0.769 vs 0.799) label fractions. Note that Rotate outperforms Scale across all 3 label fractions.

4.1.2. COMBINED AUGMENTATIONS

At the 10% and 100% label fractions, all combinations that incorporate Time Mask (with the exception of Scale + Time Mask at 100%) outperform all single augmentations. At the 10% label fraction, Rotate + Time Mask (0.786 vs 0.767), Scale + Time Mask (0.775 vs 0.767), and Rotate + Scale + Time Mask (0.795 vs 0.767) all outperform the best single augmentation performer, Rotate. At the 100% label fraction, Rotate + Time Mask (0.800 vs 0.799) and Rotate + Scale + Time Mask (0.806 vs 0.799) both outperform the best single augmentation performer, Time Mask.

Rotate + Time Mask shows improvement over all single augmentations at the 1%, 10%, and 100% label fractions. It has higher performance than the best single augmentation performer at the 1% (0.713 vs 0.703), 10% (0.786 vs 0.767), and 100% (0.800 vs 0.799) label fractions.

Rotate + Scale + Time Mask outperforms all single augmentations at the 1%, 10%, and 100% label fractions. This combination is the only combination that significantly outperforms Time Mask at all label fractions. It is also the only combination to significantly outperform Time Mask at the 100% (0.806 vs 0.799) label fraction.

4.2. Augmentation Strength

Method	PhysioNet 2020 (AUROC)		
	1% ($\mu \pm \sigma$)	10%	100%
<i>Baseline</i>			
VCG Identity	0.640 \pm 0.014	0.752	0.755
<i>Rotate</i>			
Rotate $\pm 5^\circ$	0.703 \pm 0.011*	0.767*	0.785*
Rotate $\pm 10^\circ$	0.697 \pm 0.008*	-	-
Rotate $\pm 45^\circ$	0.698 \pm 0.005*	-	-
<i>Scale</i>			
Scale 1.05	0.640 \pm 0.016	-	-
Scale 1.1	0.668 \pm 0.014*	0.738	0.769*
Scale 1.5	0.661 \pm 0.015*	-	-

Table 2: **Linear Evaluation for Different Augmentation Strengths.** * denotes statistically significant difference from VCG Identity. Experiments at the 1% fraction were run across 5 randomly drawn splits to provide an understanding of the model’s variable performance. The VCG Identity baseline applied DD^{-1} to all our ECGs as augmentations in pretraining so as to examine the effect the lossy linear transformation has on our performance.

At the 1% label fraction, we observe that Rotate outperforms VCG Identity at all augmentation strengths and that differences in performance between varying augmentation strengths are negligible. We find that the mean AUROC of Rotate $\pm 5^\circ$ (0.703), Rotate $\pm 10^\circ$ (0.697), and Rotate $\pm 45^\circ$ (0.698) are within 1 standard deviation of each other. All 3 augmentation strengths outperform VCG Identity (0.640).

At the 1% label fraction, we observe that Scale outperforms VCG Identity at stronger augmentation strengths and that differences in performance between stronger augmentation strengths are negligible. We find that the mean AUROC of Scale 1.1 (0.668) and Scale 1.5 (0.661) are within 1 standard deviation of each other. Scale 1.05 (0.640) has lower performance than Scale 1.1 and Scale 1.5. Scale 1.1 and Scale 1.5 outperform VCG Identity (0.640) while Scale 1.05 has the same performance.

Of these 3 augmentation strengths explored for each augmentation type, Rotate $\pm 5^\circ$ (0.703) and Scale 1.1 (0.668) have the best performance. We observe that Rotate $\pm 5^\circ$ outperforms VCG Identity at 1% (0.703 vs 0.640), 10% (0.767 vs 0.752), and 100% (0.785 vs 0.755). Scale 1.1 outperforms VCG Identity at 1% (0.668 vs 0.640) and 100% (0.769 vs 0.755), but does not outperform VCG Identity at 10% (0.738 vs 0.752).

4.3. Per-Pathology Performance Analysis

Classes	Best SSL Linear Eval	Supervised	Difference	Metagroup
Premature ventricular contractions	0.815 (0.784, 0.842)	0.805 (0.781, 0.829)	-0.010	large QRS basis
Pacing rhythm	0.997 (0.991, 1.000)	0.999 (0.998, 1.000)	0.002	large QRS basis
Left bundle branch block	0.954 (0.929, 0.974)	0.969 (0.949, 0.982)	0.015	large QRS basis
Left axis deviation	0.869 (0.859, 0.878)	0.897 (0.889, 0.906)	0.028	large QRS basis
Sinus rhythm	0.924 (0.919, 0.929)	0.953 (0.950, 0.957)	0.029	-
Nonspecific intraventricular conduction disorder	0.761 (0.730, 0.793)	0.797 (0.763, 0.824)	0.036	large QRS basis
T wave abnormal	0.827 (0.814, 0.839)	0.867 (0.856, 0.877)	0.040	T-wave abnormality
Left anterior fascicular block	0.893 (0.876, 0.909)	0.934 (0.921, 0.946)	0.041	large QRS basis
T wave inversion	0.773 (0.744, 0.799)	0.815 (0.792, 0.835)	0.042	T-wave abnormality
Prolonged PR interval	0.820 (0.772, 0.865)	0.863 (0.816, 0.898)	0.043	prolonged interval
Prolonged QT interval	0.867 (0.850, 0.882)	0.910 (0.894, 0.924)	0.043	prolonged interval
Complete right bundle branch block	0.896 (0.883, 0.907)	0.940 (0.930, 0.950)	0.044	large QRS basis
1st degree AV block	0.701 (0.675, 0.724)	0.751 (0.730, 0.772)	0.050	prolonged interval
Sinus bradycardia	0.920 (0.908, 0.932)	0.971 (0.964, 0.977)	0.051	-
Incomplete right bundle branch block	0.734 (0.702, 0.766)	0.787 (0.755, 0.817)	0.053	-
Sinus arrhythmia	0.585 (0.557, 0.615)	0.639 (0.602, 0.671)	0.054	-
Atrial flutter	0.868 (0.814, 0.907)	0.926 (0.897, 0.951)	0.058	-
Low QRS voltages	0.869 (0.829, 0.904)	0.933 (0.914, 0.950)	0.064	-
Right axis deviation	0.796 (0.748, 0.844)	0.869 (0.835, 0.900)	0.073	-
Atrial fibrillation	0.808 (0.791, 0.822)	0.893 (0.882, 0.904)	0.085	-
Premature atrial contraction	0.579 (0.555, 0.603)	0.670 (0.645, 0.694)	0.091	-
Q wave abnormal	0.684 (0.650, 0.723)	0.795 (0.772, 0.818)	0.111	-
Sinus tachycardia	0.720 (0.700, 0.739)	0.834 (0.820, 0.847)	0.114	-
Bradycardia	0.696 (0.658, 0.737)	0.833 (0.811, 0.858)	0.137	-

Table 3: **Per-Diagnosis AUROC Comparisons.** We compare the linear evaluation of our best self-supervised learning model (Rotate + Scale + Time Mask) with a fully supervised, randomly-initialized model, both trained on 100% of labels. The 95% confidence interval is reported with each AUROC, and the table is sorted by mean difference between the fully supervised model and the best self-supervised model.

By examining groupings of the diagnoses and their relative performance in a post-hoc analysis, it may be possible to better understand how our physiologically-inspired self-supervised learning scheme compares to a fully supervised approach. There were three possible diagnostic categories for which our approach performed the closest to fully supervised learning (heuristically determined to be a < 0.05 AUROC difference):

- **Diagnoses based on large QRS changes:** Diagnoses in this category are based on larger-scale QRS perturbations, relative to other diagnoses. Because of the spatial nature of making diagnoses in this metagroup, spatially-aware, signal-preserving augmentations like VCG rotations may provide a useful augmentation in a self-supervised setup.
- **Prolonged intervals:** Diagnoses based on prolongation of intervals between discrete ECG waveforms. Because of the temporal nature of diagnoses in this metagroup, spatial VCG augmentations can be applied to produce gains in a self-supervised setup while preserving the group’s main invariances.
- **T-wave abnormalities:** Abnormalities in the T-wave section of the waveform. Temporal augmentations like time mask would force a self-supervised learning model to place more weight on beat-level T-wave abnormalities, helping close the gap on a fully-supervised setup even in a linear evaluation setting.

Except for sinus rhythm, which is the most common diagnosis, diagnoses that approached fully-supervised performance could be classified post-hoc into several metagroups. These groupings are loosely defined and determined post-hoc. We hypothesize, however, that the diagnoses based on large QRS changes may benefit from the VCG augmentations in particular, given their reliance on relative spatial relationships. We also hypothesize that Sinus may approach fully-supervised performance in a self-supervised learning setup due to its status the most common diagnosis.

5. Discussion

In this work, we explore the effectiveness of physiologically inspired augmentations for representation learning of ECGs.

We show that physiologically inspired augmentations of ECG signals can be leveraged to learn stronger representations of ECG signals. Our findings suggest that applying spatiotemporal perturbations to bio-signals can make for strong augmentations in a contrastive learning setup. Previous work that have necessitated representation learning of bio-signals have considered patient metadata (Vu et al., 2021) and MoCo pretraining (Sowrirajan et al., 2021), but to the best of our knowledge none have considered physiologically inspired augmentations. Furthermore, our findings on the augmentation strength of physiologically inspired augmentations do not contradict those of Tian et al. (2020). Specifically, Tian et al. (2020) finds that the performance of a model with respect to augmentation strength traces out a reverse U-shape. Although our findings indicate that varying the augmentation strengths for physiologically inspired augmentations does not substantially change the performance, we observe that the slight changes in performance could potentially trace out a reverse U-shape, perhaps if more augmentation strengths were tested.

We show that the combination of physiologically inspired and temporal augmentations can be leveraged to learn representations that are stronger than those learned by any single augmentation type. Specifically, our finding that the combination of 3 augmentations (both physiologically inspired and temporal) is the only combination that results in significantly higher performances across all data labeling regimes is a strong indicator of this. It suggests

that combining augmentations derived in different manners for bio-signals could increase the diversity of features learned by representations, and hence the performance. This is inline with the findings of [Chen et al. \(2020b\)](#), which showed that the combination of augmentations in a contrastive learning setup could amount to gains in performance greater than the gains in performance of any individual augmentation.

Limitations Some limitations to this paper should be noted. First, this work does not do an exhaustive hyperparameter search to determine the ideal time mask percentage, rotation, and scale amounts. Moreover, because the purpose of this work was to demonstrate the value of biomedically derived augmentations within one framework, we do not compare against other self-supervised frameworks for ECG interpretation. Similarly, we also did not leverage semi-supervised techniques such as knowledge distillation in our pipeline. Even though our dataset was comprised of multiple independent sets of ECG recordings collected all over the world, we did not explore the effect of VCG augmentations on learning each individual data source. Finally, we did not formally investigate the relationship between encoder size and performance, instead opting to use a relatively small network in both pretraining and fine-tuning due to computing resource constraints.

References

Erick A Perez Alday, Annie Gu, Amit J Shah, Chad Robichaux, An-Kwok Ian Wong, Chengyu Liu, Feifei Liu, Ali Bahrami Rad, Andoni Elola, Salman Seyed, Qiao Li, Ashish Sharma, Gari D Clifford, and Matthew A Reyna. Classification of 12-lead ecgs: the physionet/computing in cardiology challenge 2020. *Physiological Measurement*, 2020. URL <http://iopscience.iop.org/article/10.1088/1361-6579/abc960>.

Daejoon Anh, Subramaniam Krishnan, and Frank Bogun. Accuracy of electrocardiogram interpretation by cardiologists in the setting of incorrect computer analysis. *Journal of electrocardiology*, 39(3):343–345, 2006.

Zachi I Attia, Suraj Kapa, Francisco Lopez-Jimenez, Paul M McKie, Dorothy J Ladewig, Gaurav Satam, Patricia A Pellikka, Maurice Enriquez-Sarano, Peter A Noseworthy, Thomas M Munger, et al. Screening for cardiac contractile dysfunction using an artificial intelligence–enabled electrocardiogram. *Nature medicine*, 25(1):70–74, 2019a.

Zachi I Attia, Peter A Noseworthy, Francisco Lopez-Jimenez, Samuel J Asirvatham, Abhishek J Deshmukh, Bernard J Gersh, Rickey E Carter, Xiaoxi Yao, Alejandro A Rabinstein, Brad J Erickson, et al. An artificial intelligence-enabled ecg algorithm for the identification of patients with atrial fibrillation during sinus rhythm: a retrospective analysis of outcome prediction. *The Lancet*, 394(10201):861–867, 2019b.

Alexei Baevski, Henry Zhou, Abdelrahman Mohamed, and Michael Auli. wav2vec 2.0: A framework for self-supervised learning of speech representations, 2020.

RR Bond, Tingting Zhu, DD Finlay, B Drew, PD Kligfield, Daniel Guldenring, Cathal Breen, AG Gallagher, MJ Daly, and GD Clifford. Assessing computerized eye tracking technology for gaining insight into expert interpretation of the 12-lead electrocardiogram: an objective quantitative approach. *Journal of electrocardiology*, 47(6):895–906, 2014.

Andrew W Cairns, Raymond R Bond, Dewar D Finlay, Daniel Guldenring, Fabio Badilini, Guido Libretti, Aaron J Peace, and Stephen J Leslie. A decision support system and rule-based algorithm to augment the human interpretation of the 12-lead electrocardiogram. *Journal of electrocardiology*, 50(6):781–786, 2017.

Ting Chen, Simon Kornblith, Mohammad Norouzi, and Geoffrey Hinton. A simple framework for contrastive learning of visual representations, 2020a.

Ting Chen, Simon Kornblith, Kevin Swersky, Mohammad Norouzi, and Geoffrey Hinton. Big self-supervised models are strong semi-supervised learners, 2020b.

Xinlei Chen, Haoqi Fan, Ross Girshick, and Kaiming He. Improved baselines with momentum contrastive learning, 2020c.

Joseph Y. Cheng, Hanlin Goh, Kaan Dogrusoz, Oncel Tuzel, and Erdrin Azemi. Subject-aware contrastive learning for biosignals, 2020.

W Einthoven, G Fahr, and A De Waart. On the direction and manifest size of the variations of potential in the human heart and on the influence of the position of the heart on the form of the electrocardiogram. *American heart journal*, 40(2):163–211, 1950.

Francis M Fesmire, Robert F Percy, Jim B Bardoner, David R Wharton, and Frank B Calhoun. Usefulness of automated serial 12-lead ecg monitoring during the initial emergency department evaluation of patients with chest pain. *Annals of emergency medicine*, 31(1):3–11, 1998.

Jean-Bastien Grill, Florian Strub, Florent Altché, Corentin Tallec, Pierre H. Richemond, Elena Buchatskaya, Carl Doersch, Bernardo Avila Pires, Zhaohan Daniel Guo, Mohammad Gheshlaghi Azar, Bilal Piot, Koray Kavukcuoglu, Rémi Munos, and Michal Valko. Bootstrap your own latent: A new approach to self-supervised learning, 2020.

Kaiming He, Haoqi Fan, Yuxin Wu, Saining Xie, and Ross Girshick. Momentum contrast for unsupervised visual representation learning, 2020.

R Devon Hjelm, Alex Fedorov, Samuel Lavoie-Marchildon, Karan Grewal, Phil Bachman, Adam Trischler, and Yoshua Bengio. Learning deep representations by mutual information estimation and maximization, 2019.

J Willis Hurst. Methods used to interpret the 12-lead electrocardiogram: Pattern memorization versus the use of vector concepts. *Clinical cardiology*, 23(1):4–13, 2000.

Rene Jaros, Davide Radek Martinek, and Lukas Danys. Comparison of different electrocardiography with vectocardiography transformations. *Sensors*, 19(14), July 2019. doi: 10.3390/s19143072. URL <https://dx.doi.org/10.3390%2Fs19143072>.

Anthony H. Kashou, Hajira Basit, and Lovely Chhabra. *Electrical Right and Left Axis Deviation*. StatPearls Publishing, June 2020.

Harold L. Kennedy. Ambulatory (holter) electrocardiography technology. *Cardiology Clinics*, 10(3):341–359, 1992. ISSN 0733-8651. doi: [https://doi.org/10.1016/S0733-8651\(18\)30218-2](https://doi.org/10.1016/S0733-8651(18)30218-2). URL <https://www.sciencedirect.com/science/article/pii/S0733865118302182>. Ambulatory Electrocardiography: Current Clinical Concepts.

Diederik P. Kingma and Jimmy Ba. Adam: A method for stochastic optimization, 2017.

Dani Kiyasseh, Tingting Zhu, and David A. Clifton. CloCS: Contrastive learning of cardiac signals across space, time, and patients, 2020a.

Dani Kiyasseh, Tingting Zhu, and David A. Clifton. Drops: Deep retrieval of physiological signals via attribute-specific clinical prototypes, 2020b.

Dani Kiyasseh, Tingting Zhu, and David A. Clifton. PCPs: Patient cardiac prototypes, 2020c.

Giorgio Olivetti, Giovanna Giordano, Domenico Corradi, Massimo Melissari, Costanza Lagrasta, Steven R Gambert, and Piero Anversa. Gender differences and aging: effects on the human heart. *Journal of the American College of Cardiology*, 26(4):1068–1079, 1995.

Stephen M Salerno, Patrick C Alguire, and Herbert S Waxman. Competency in interpretation of 12-lead electrocardiograms: a summary and appraisal of published evidence. *Annals of Internal Medicine*, 138(9):751–760, 2003.

Pritam Sarkar and Ali Etamad. Self-supervised learning for ecg-based emotion recognition, 2019.

Hari Sowrirajan, Jingbo Yang, Andrew Y. Ng, and Pranav Rajpurkar. Moco-cxr: Moco pretraining improves representation and transferability of chest x-ray models, 2021.

Yonglong Tian, Dilip Krishnan, and Phillip Isola. Contrastive multiview coding, 2019.

Yonglong Tian, Chen Sun, Ben Poole, Dilip Krishnan, Cordelia Schmid, and Phillip Isola. What makes for good views for contrastive learning?, 2020.

Geoffrey H Tison, Jeffrey Zhang, Francesca N Delling, and Rahul C Deo. Automated and interpretable patient ecg profiles for disease detection, tracking, and discovery. *Circulation: Cardiovascular Quality and Outcomes*, 12(9):e005289, 2019.

Aaron van den Oord, Yazhe Li, and Oriol Vinyals. Representation learning with contrastive predictive coding, 2018.

Yen Nhi Truong Vu, Richard Wang, Niranjan Balachandar, Can Liu, Andrew Y. Ng, and Pranav Rajpurkar. Medaug: Contrastive learning leveraging patient metadata improves representations for chest x-ray interpretation, 2021.

Zhirong Wu, Yuanjun Xiong, Stella Yu, and Dahua Lin. Unsupervised feature learning via non-parametric instance-level discrimination, 2018.